Supporting Information

Facile Synthesis of Tetraphenylpyrazine-Based AIE Molecules with distinguishable Fluorescence for Aging Latent Fingerprint Visualization

Ping Yang, * Yuanlin Zhang, Wen Liu, Kuiliang Li*, Duoduo Hu and Haoyuan Lv

Table of Contents

1.General Information

4-Bromobenzaldehyde, ethanol, triethylamine, ammonium acetate, acetic anhydride, acetic acid, 1-bromopentane, sodium iodide, acetone, 4-aminophenylboronic acid pinacol ester, N, N-dimethylformamide, sodium sulfate, tetra(triphenylphosphine)palladium, potassium carbonate, and 1,4-dioxane were purchased from Shanghai McLean Biochemical Technology Co., Ltd. All reagents used were of analytical grade. The nuclear magnetic resonance (NMR) spectrometer used was an Ascend Evo 400 (Bruker, unless otherwise specified). The Fourier transform infrared (FT-IR) spectrometer was a model IR Racer-100. Photoluminescence (PL) spectra were acquired using a Hitachi F-4600 Fluorescence Spectrometer. High-resolution mass spectra (HRMS) were recorded on a P-SIMS-Gly instrument (Bruker Daltonics Inc.) via electrospray ionization-time of flight (ESI-TOF) mode. Commercially available compounds were used without further purification. All solvents were purified according to standard procedures unless otherwise noted.

2.Synthesis of TPP-APBP-P molecule

2.1 Preparation of TPP-4Br molecule

In a 100 mL flask, 4-Bromobenzaldehyde (12.10 g, 60.0 mmol) and VB1 (1.01 g, 3.0 mmol) were mixed with ethanol (40.0 mL) and triethylamine (2.5 mL, 18.0 mmol). The suspension was stirred under N_2 at 80°C for 24 hours. After the reaction, the suspension was concentrated, extracted, washed, dried, and purified by column chromatography (petroleum ether: ethyl acetate = 4:1) to yield compound 1 (7.99 g, 21.60 mmol, 72%). Compound 1 (4.80 g, 12.97 mmol), ammonium acetate (3.12 g, 40.50 mmol), and acetic anhydride (2.5 mL, 26.44 mmol) were added to a 100 mL flask, dissolved in acetic acid, and refluxed at 130°C for 12 hours. After the reaction was completed, the mixture was cooled to room temperature, filtered, and washed with acetic acid to obtain the yellow solid powder TPP-4Br molecule (1.67 g, 2.38 mmol, 37%).

2.2 Preparation of APBP-P molecule

1-Bromopentane (15.10 g, 100.0 mmol) and sodium iodide (22.48 g, 150.0 mmol) were dissolved in 50 mL of acetone and stirred at room temperature for half an hour, yielding a white precipitate. The mixture was concentrated, extracted, washed, and dried to produce colorless oily 1-Iodopentane (10.62 g, 53.60 mmol, 70.3%). 1-Iodopentane (5.94 g, 30 mmol) and 4-Aminophenylboronic acid pinacol ester (4.38 g, 20 mmol) were dissolved in 50 mL DMF with a catalytic amount of sodium sulfate and refluxed at 70°C for 3 hours. When the reaction ended, the solution was cooled to room temperature, concentrated, extracted,

washed, and dried, and then purified by column chromatography (petroleum ether: ethyl acetate = 10:1). Finally, a yellow oily APBP-P molecule (1.80 g, 6.22 mmol, 41.1%) was obtained.

2.3 Preparation of TPP-APBP-P molecule

TPP-4Br molecule (1.4 g, 2 mmol) and APBP-P molecule (1.74 g, 6 mmol) were dissolved in a mixed solvent (1,4-dioxane: H_2O = 10:1). A catalytic amount of tetra(triphenylphosphine)palladium and potassium carbonate were added, and the mixture was refluxed under N^2 protection at 100°C for 12 hours. After the reaction, the solution was cooled, extracted with dichloromethane, concentrated, washed, dried, and purified by column chromatography (petroleum ether: ethyl acetate = 3:1) to yield the yellow solid TPP-APBP-P molecule (0.62 g, 0.61 mmol, 44.6%). The 1H NMR spectrum (400 MHz, DMSO-d6) exhibited peaks at δ 7.80 – 7.73 (m, 1H), 7.67 – 7.52 (m, 15H), 7.49 – 7.44 (m, 3H), 7.40 – 7.36 (m, 1H), 6.72 – 6.54 (m, 4H), 5.83 (s, 2H), 3.16 – 2.85 (m, 4H), 1.59 – 1.51 (m, 4H), 1.38 – 1.32 (m, 8H), 0.91 – 0.85 (m, 6H).

3.^{1}HNMR Spectra, IR and HRMS

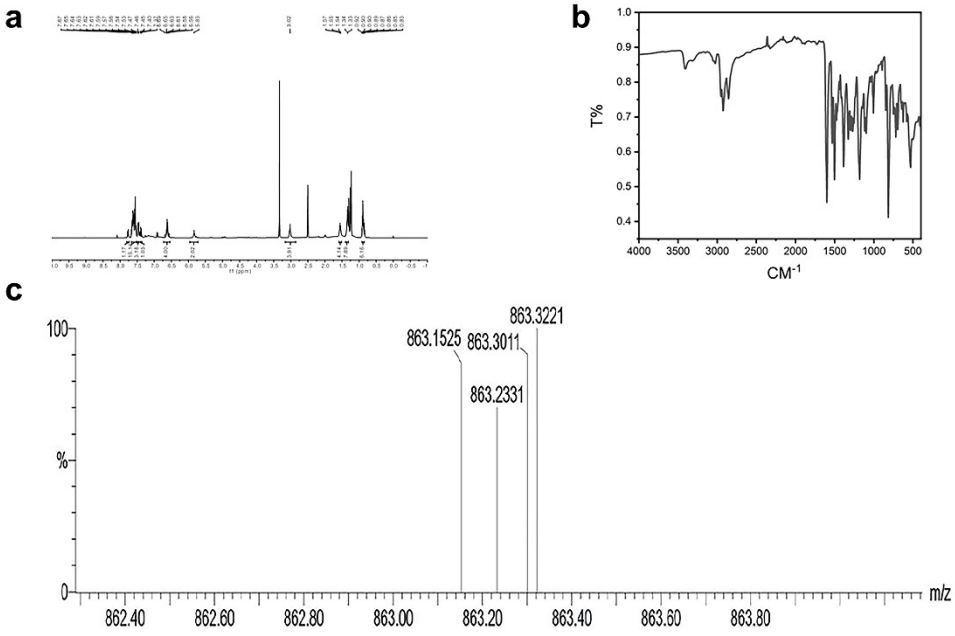

Fig. S1 (a) TPP-APBP-P 1H NMR plot; (b) TPP-APBP-P infrared spectral plot; (c) High-resolution mass spectra of TPP-APBP-P

As shown in Fig. S1a, the signals in the 1H NMR spectrum are assigned as follows: δ 6.72-6.54 (m, 4H) corresponds to the aromatic hydrogens (Hg) on the benzene ring adjacent to the amino group; δ 5.83 (s, 2H) represents the exchangeable hydrogens (Hf) on the amino nitrogen; δ 3.16-2.85 (m, 4H) is attributed to He; δ 1.59-1.51 (m, 4H) corresponds to Hd; δ 1.38-1.32 (m, 8H) is assigned to Hb and Hc; δ 0.91-0.85 (m, 6H) corresponds to Ha. The remaining aromatic hydrogens on the benzene rings are observed at δ 7.80-

7.73 (m, 1H), 7.67-7.52 (m, 15H), 7.49-7.44 (m, 3H), and 7.40-7.36 (m, 1H). Fig. S1b displays the infrared (IR) spectrum of TPP-APBP-P. The peak around 3400 cm^{-1} is attributed to the N-H bond, the peak near 3000 cm^{-1} corresponds to aromatic C-H bonds, the two peaks around 1500 cm^{-1} are assigned to the benzene ring and C-N bonds, and the peak at approximately 800 cm^{-1} arises from the para-substituted benzene ring. Fig. S1c presents the high-resolution mass spectrum (HRMS) of TPP-APBP-P, with a measured peak at 863.2331 closely aligning with the theoretical value of 863.2138, confirming the molecular structure's accuracy.

4.Photoluminescence spectra

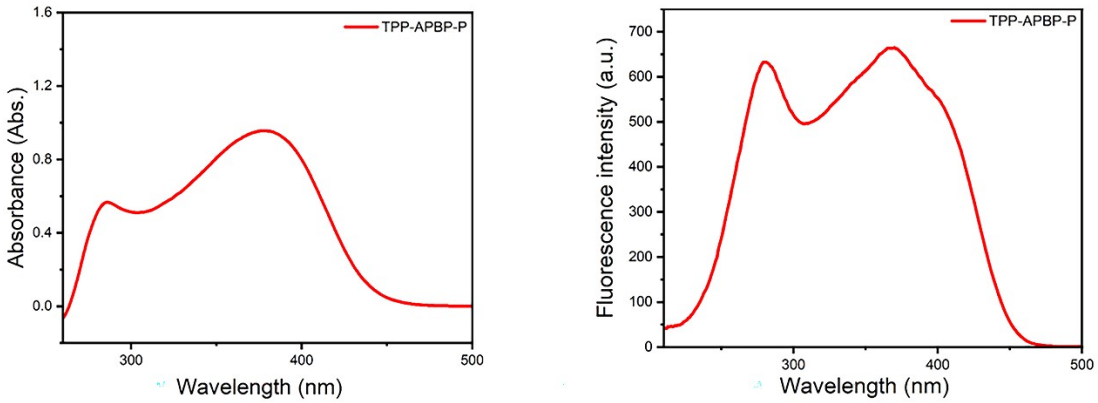

Fig. S2 The absorbance spectrum and excitation spectrum of 1.0×10^{-7} mM TPP-APBP-P molecule.

5.The quantum yield and the Fluorescence photograph of spectra.

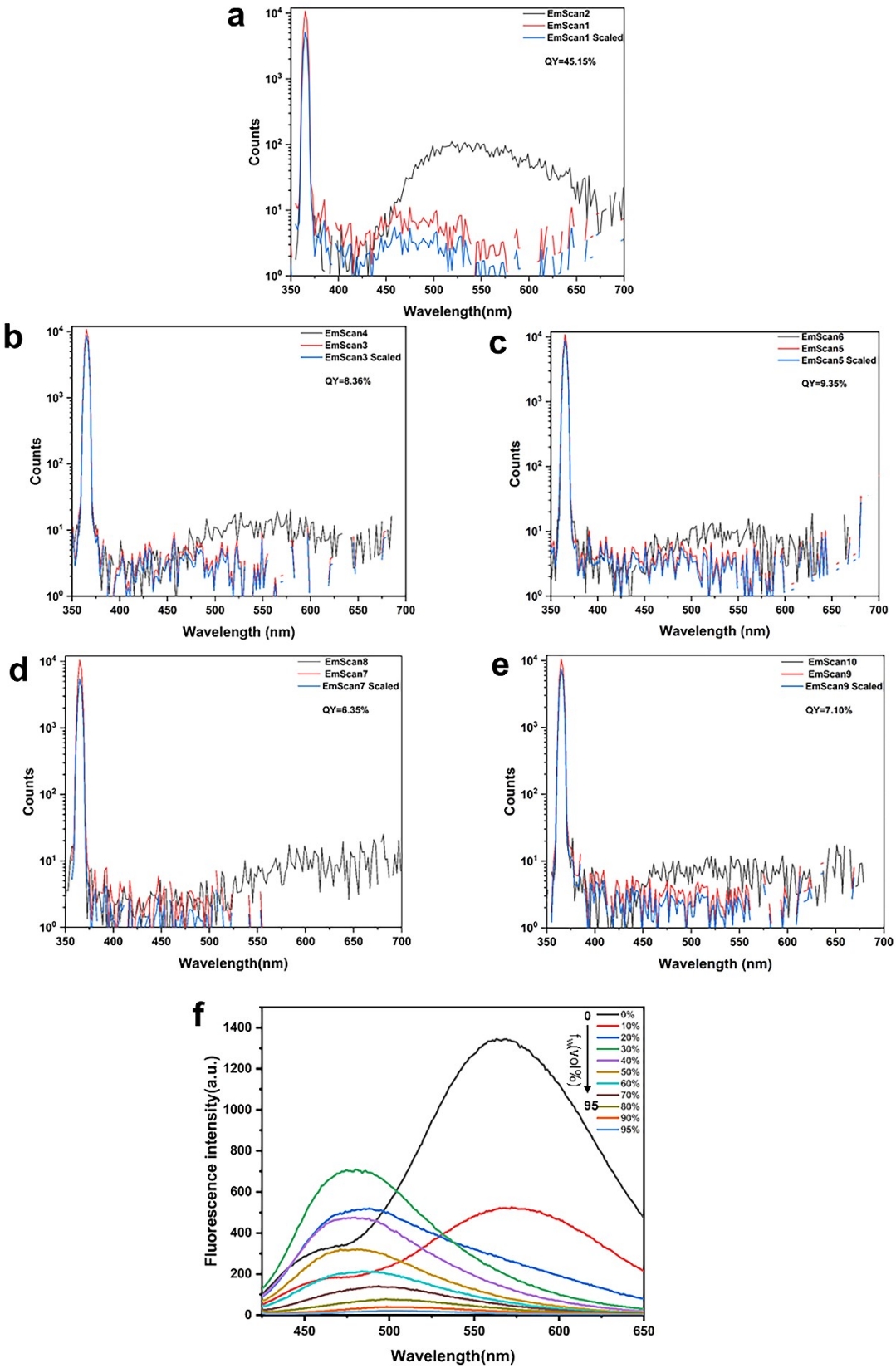

Fig. S3 (a) the quantum yield was 45.15% for H_2O: THF = 0:10; (b) the quantum yield was 8.36% for H_2O: THF = 5:5; (c) the quantum yield was 9.35% for H_2O: THF = 6:4; (d) the quantum yield was 6.25% for H_2O: DMF = 8:2; (e) the quantum yield was 7.10% for H_2O: DMF = 7:3; (f) Fluorescence photograph of spectra of

TPP-APBP-P (1.0×10^{-7} mM) in DMF/H_2O mixtures with different fw.

6.DLS

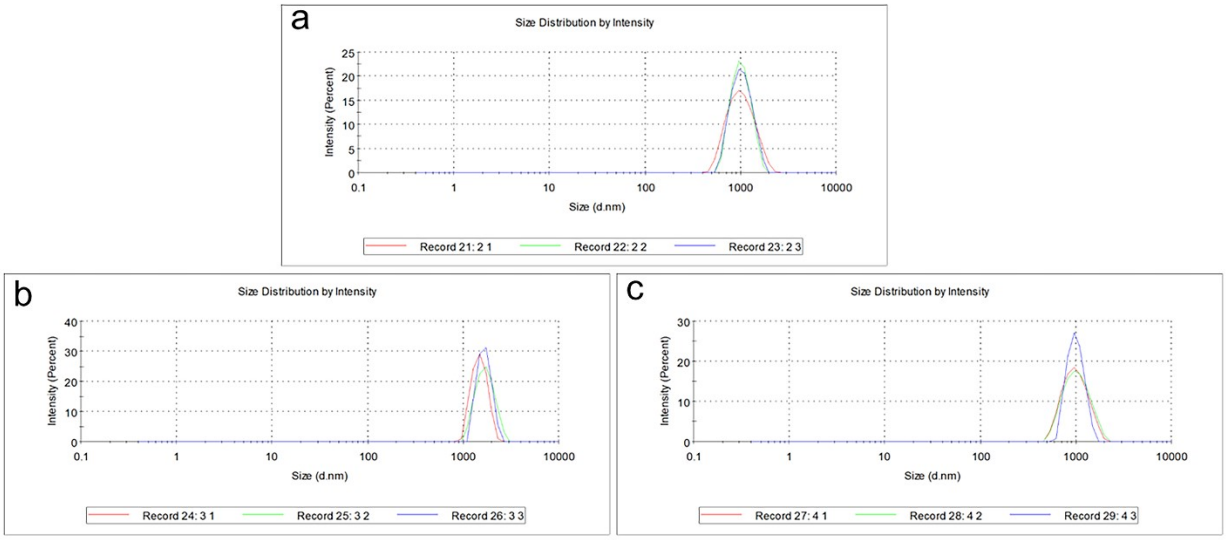

Fig. S4 (a) DLS spectrum of TPP-APBP-P at 50 % water fraction; (b) DLS spectrum of TPP-APBP-P at 60 % water fraction; (c) DLS spectrum of TPP-APBP-P at 70 % water fraction.

7.X-ray diffraction (XRD) patterns of TPP powder and TPP-APBP-P powder

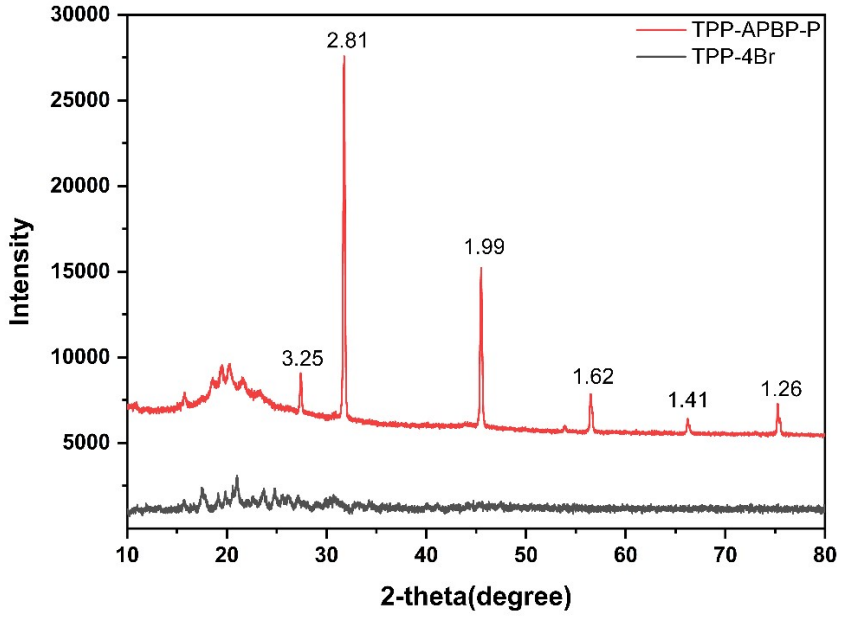

Fig. S5 X-ray diffraction (XRD) patterns of TPP powder and TPP-APBP-P powder.

8.Fingerprint images on different substrates under a biological microscope

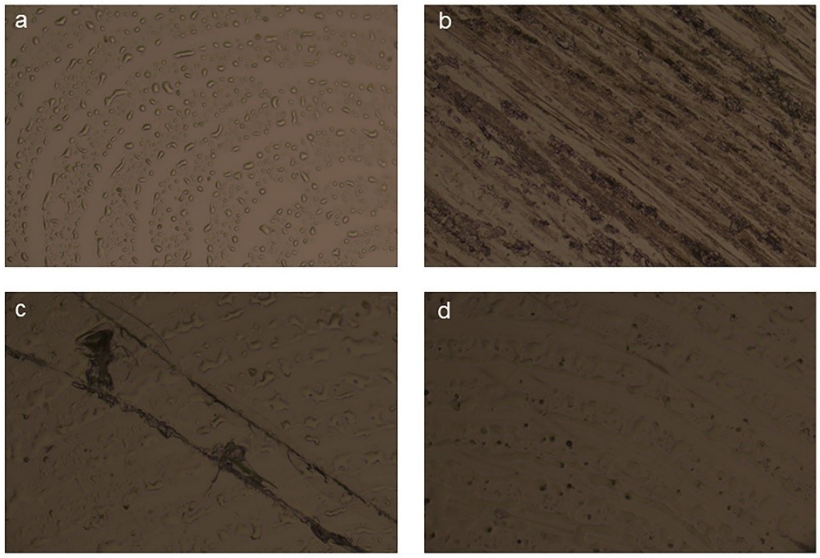

Fig. S6 (a) Fingerprint development on a smooth glass slide; (b) Fingerprint development on a frosted glass slide; (c) and (d) Fingerprint development on glass slides with varying degrees of scratches.

From the perspective of hydrophobicity, highly hydrophobic surfaces (e.g., polypropylene plastic) exhibit better compatibility with lipophilic compounds. This is because lipids are more readily adsorbed through hydrophobic interactions, leading to clearer fingerprint development. In contrast, aluminum foil surfaces-typically treated with hydrophobic coatings (e.g., silicon or wax)-hinder the uniform adhesion of developing reagents and impede their reactions with fingerprint residues. Regarding porosity, porous materials (e.g., porcelain boats) absorb liquid lipids via capillary action, causing the diffusion of fingerprint ridges and a subsequent reduction in imaging resolution. Non-porous surfaces (e.g., glass slides, coins), however, restrict the lateral migration of lipids, thereby better preserving the morphological details of fingerprints. In terms of roughness, smooth surfaces (e.g., polished stainless steel, glass slides, ceramic tiles) enable the display of continuous fingerprint ridge patterns, facilitating the complete development of latent fingerprints [1].

In this study, biological microscopy was employed to analyze fingerprint residues on surfaces with varying characteristics, and the corresponding results are presented in Fig. S6 of the Supporting Information (SI). Specifically, experiments were conducted using scratched slides, frosted glass slides, and intact smooth slides to investigate the effects of surface roughness, porosity, and hydrophobicity on fingerprint imaging. The smooth slides (Fig. S6a) clearly display complete ridge patterns-aligning with the roughness-related mechanism that smooth

surfaces allow for continuous ridge presentation, resulting in more comprehensive fingerprint development by restricting lipid migration. As shown in Fig. S6b, frosted slides exhibit incomplete presentation of fingerprint ridge patterns: consistent with the porosity-related principle discussed earlier, porous materials (e.g., porcelain boats) absorb liquid lipids via capillary action, leading to ridge diffusion and reduced imaging resolution. Additionally, Fig. S6c and S6d simulate the texture of coin substrates using slides with different scratch levels; these results reveal that surface irregularities do not compromise the overall visualization of fingerprints.

9.Contact angle measurement

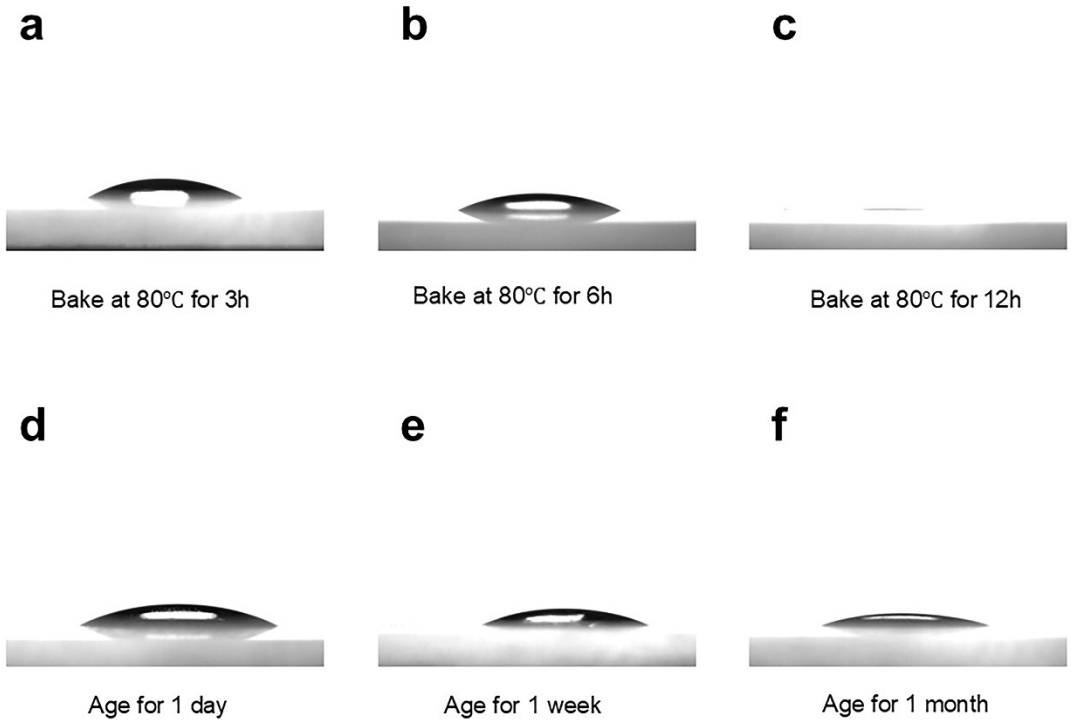

Fig. S7 (a) Contact angle under 80°C baking for 3 hours; (b)Contact angle under 80°C baking for 6 hours; (c) Contact angle under 80°C baking for 12 hours; (e)Contact angle after aging for one day; (f)Contact angle after aging for one week; (g)Contact angle after aging for one month.

The interaction mechanism between TPP-APBP-P molecules and fingerprint residues is primarily based on physical adsorption, following the "like dissolves like" principle. Sebaceous components in fingerprint residues (e.g., triglycerides, fatty acids, wax esters) are non-polar organic substances that bind to lipophilic AIE compounds via hydrophobic interactions. This selective enrichment on fingerprint ridges enables visualization under UV light. However, lipophilic components undergo dynamic desorption and chemical transformation through processes such as volatilization, oxidative decomposition, phase transition, and matrix effects-collectively leading to an exponential decay in detectable sebum characteristic signals over time.

This study verified the variation in lipid content through contact angle measurements. The specific experimental

procedure is as follows: Volunteers pressed their fingers onto glass slides to leave fingerprints. A micro syringe was used to dispense small water droplets on the surface of the fingerprint samples, and after the droplets stabilized, a high-resolution camera was employed to capture their lateral profiles. As shown in Fig. S7a-7c, the contact angle of the fingerprints gradually decreased after high-temperature baking for 3, 6, and 12 hours. Fig. S7d-7f also indicates that the contact angle continued to decrease with the extension of fingerprint aging time. All the above results confirm that the lipid content in the residues gradually decreases.

Reference

1. S. Bera, A. Selvakumaraswamy, B. P. Nayak and P. Prasad, *Chem. Commun.*, 2024, **60**, 8314-8338.